Volume 1 | Number 1 | Jan 2013 | Pages 1–100

Journal of
Materials Chemistry C

Materials for optical and electronic devices
www.rsc.org/materialsC

ROYAL SOCIETY
OF CHEMISTRY

ROYAL SOCIETY
OF CHEMISTRY

www.rsc.org/materialsC

ARTICLE

Cellulose - spin crossover particle composite papers with reverse printing performance: A proof of concept

V. Nagy,[a] I. Suleimanov.[b,c] G. Molnár,[b] L. Salmon,[b] A. Bousseksou,[b,*] and L. Csóka[a,*]

We report on a thermochromic paper with reverse printing performance. The paper was elaborated by combining spin-crossover particles of [Fe(NH$_2$trz)$_3$]Br$_2$ or [Fe(Htrz)$_2$(trz)]BF$_4$ and linter cellulose fibers using standard paper-making processes. The composites were characterized by electronic and vibrational spectroscopies, thermogravimetry, calorimetry, tensile tests, elemental analyses as well as by electronic and optical microscopies. The composite cellulose sheets keep good mechanical and thermal properties and show perceptible thermochromic effects associated with a memory effect. They are rewritable by laser heating and completely erasable over several hundreds of printing cycles providing scope for inkless printing technologies.

Introduction

The renewable and sustainable natural polymer, cellulose, has been used for centuries as a basic medium and template for the ink based printing technology [1]. Cellulose has been researched for great many decades and found still applicable, but not replaceable in presenting information. Ink based (not erasable) printing technology has developed tremendously through technological revolutions from the 14th century for transmitting and conveying information on reading materials in human communication and promote literacy on paper substrates. In the printing process the text or images are transferred from an inked template to a cellulose substrate, basically in irreversible way. This fact brings about serious environmental, sustainability and economic issues, including deforestation and chemical pollution. Rewritable paper using inkless printing is an attractive alternative with significant economic potential and huge environmental advantages. Up to now mainly photochromic or redox dyes or chemical developer (e.g. water, acids, etc.) induced reversible color changes have been tested to this aim, though propositions based on other photonic principles (e.g. diffraction) have been also published [2-14]. However, none of these ideas could really meet industry demands, either due to the low performance and instability of the dye or its technological (or economical) incompatibility with standard papermaking technologies.

Here we report a proof of concept of developing a reversible, inkless, printable substrate from cellulose/spin crossover (SCO)

composites [15]. These latter are transition metal complexes, well-known for their thermochromic properties associated with the high spin (HS) – low spin (LS) spin state switching phenomenon [16]. For certain complexes the thermochromism is accompanied by a large thermal hysteresis, which provides scope for storing printed information in these compounds [17]. The information or characters are developed by heating or cooling the carrier cellulose substrate without using any chemical compound or ink. To the best of our knowledge, this is the first time to achieve a reversible, rewritable, erasable, contactless thermal printing of cellulose substrate to use as a short or long term memory device.

Materials and methods

Bleached linter cellulose fibers were received from Buckeye Technologies Inc. Htrz (1,2,4-triazole) was received from Alfa Aesar. FeBr$_2$, Fe(BF$_4$)$_2$.6H$_2$O and NH$_2$trz (4-amino-1,2,4-triazole) were received from Sigma Aldrich.

Synthesis of the SCO complexes

For the synthesis of the SCO complex [Fe(Htrz)$_2$(trz)]BF$_4$ [18] (**1**) two distinct solutions were prepared: 1) Fe(BF$_4$)$_2$.6H$_2$0 (113 mg, 0.3 mmol, 1 unit) in a solvent (1 ml, H2O); 2) 1,2,4-triazole (69 mg, 0.9 mmol, 3 units) in a solvent (0.5 ml EtOH). The two solutions were rapidly mixed and the mixture became turbid within a few minutes followed by the establishment of a pink-purple precipitate. The precipitate was separated by centrifugation and washed twice with water. The [Fe(Htrz)$_2$(trz)]BF$_4$ particles obtained by this method showed a size distribution between ca. 1-5 μm (Figure 1). Pyrene luminophore grafted [Fe(Htrz)$_2$(trz)]BF$_4$ particles were synthesized as decribed in ref. [19]. For the synthesis of the SCO complex [Fe(NH$_2$trz)$_3$]Br$_2$ [20] (**2**) two distinct solutions were prepared: 1) FeBr$_2$ (46 mg, 0.2 mmol, 1 unit), ascorbic acid (15 mg) in a solvent (1 ml, H2O); 2) NH$_2$trz (54 mg, 0.6 mmol, 3 units) in a solvent (0.5 ml,

[a.] University of West Hungary, Institute of Wood Based Products and Technologies, 9400 Sopron, Hungary.
[b.] Laboratoire de Chimie de Coordination, CNRS & Université de Toulouse (UPS, INPT), Toulouse, France.
[c.] Department of Chemistry, Taras Shevchenko National University of Kyiv, Kyiv 01601, Ukraine.

This journal is © The Royal Society of Chemistry 20xx

J. Mat. Chem. C, 2015, **00**, 1-3 | **1**

ARTICLE   *Journal of Materials Chemistry C*

H_2O). The two solutions were rapidly mixed and the mixture became turbid within a few minutes followed by the establishment of a pink-purple precipitate. The precipitate was separated by centrifugation. The $[Fe(NH_2trz)3]Br_2$ particles obtained by this method showed a size distribution between ca. 400-1000 nm (Figure 1).
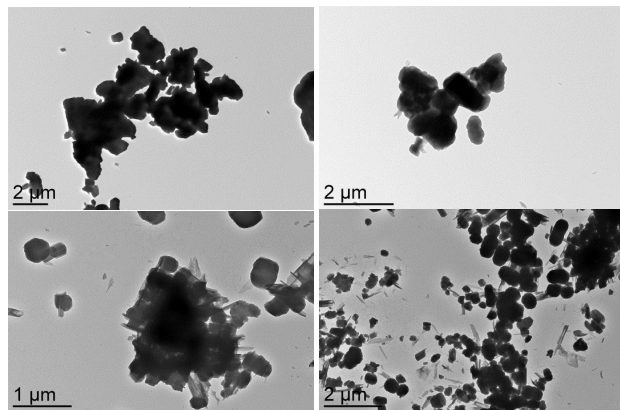

Figure 1. TEM images of as-prepared $[Fe(Htrz)_2(trz)]BF_4$ (upper panel) and $[Fe(NH_2trz)3]Br_2$ (lower panel) particles

Synthesis of the SCO/cellulose composites

For the preparation of composite **1** first a suspension of $[Fe(Htrz)_2(trz)]BF_4$ (100 mg in 2 ml of ethanol+H_2O 1:2) with 100 mg ascorbic acid was prepared by ultrasonication. This was then added to a water suspension of linter cellulose fibers (140 mg of fibers in 10 ml of H_2O) and further sonicated. The iron content of the resulting centrifuged composite was 3.9 w%, from which the adsorbed amount of the complex was estimated to ca. 25 w%. For the preparation of composite **2**, first a suspension of $[Fe(NH_2trz)_3]Br_2$ (100 mg in 4 ml of ethanol) was prepared by 3 min ultrasonication. This suspension was then added to an ethanol suspension of linter cellulose fibers (140 mg of fibers in 10 ml of ethanol) and further sonicated. The iron content of the resulting centrifuged composite was 3.5 w%, from which the adsorbed amount of the complex was estimated to ca. 30 w%. Handsheets of modified pulps were made with a basis weight of 100 g/m2 by means of a HAAGE D-4330 Systems laboratory sheet former according to DIN EN ISO 5269-2. After filtration and drying, the samples (modified and unmodified cellulose fiber sheets) were conditioned at 50 % relative humidity and a temperature of 23 °C.

Electron microscopy

A HITACHI S-3400N instrument was used for scanning electron microscopy (SEM) imaging of both modified and unmodified cellulose sheets. The images were obtained at an operating voltage of 17 kV in backscattered electron mode. The SCO particles were imaged by transmission electron microscopy (TEM) by means of a JEOL JEM-1010 (100 kV) microscope. TEM samples were prepared by deposition of the particle suspension on a carbon-coated copper microscopy grid.

Inductively coupled plasma-atomic emission spectrometry (ICP-AES)

An iCAP 6300 (Thermo Fisher Scientific) instrument was used to determine the amount of iron in the cellulose sheets following microwave digestion in a HNO_3 (65 %) / H_2O_2 (30 %) mixture.

Electronic and vibrational spectroscopies

UV/VIS diffuse reflection spectra were recorded in ambient conditions on a Lambda-35 spectrophotometer (Perkin Elmer) equipped with an integrating sphere. The CIELab coordinates were determined at room temperature using an Elrepho (AB Lorentzen and Wettre) Paper Brigthness/Opacity/Color Testing Instrument. IR spectra were recorded on a Spectrum-100 (Perkin Elmer) FTIR instrument in ATR mode in ambient conditions between 600-4000 cm^{-1} with a resolution of 4 cm^{-1}. Raman spectra were collected in the 100-2300 cm^{-1} frequency range using an Xplora (Horiba) Raman microspectrometer (spectral resolution ca. 3 cm-1). The 638 nm line of a diode laser was focused on the sample using a 0.5 NA numerical aperture objective. The laser power was adjusted between 0.1 and 3 mW. Spectra were recorded in air and the sample temperature was controlled using a Peltier stage (Linkam Scientific Instruments, LTS120).

Optical microscopy

Variable temperature optical reflectance microscopy images were acquired using a MOTIC SMZ-168 stereomicroscope equipped with a MOTICAM 1000 color camera operated in the green spectral range (around 540 nm). For both composites, the temperature during microscopy observation was controlled at a rate of 2 °C/min using the LTS120 stage. Variable temperature fluorescence microscopy images were acquired at a rate of 4 °C/min using an Olympus BX51 microscope equipped with a Peltier-cooled CCD camera (Andor Technology IkonM). The excitation (450 nm) and emission (550 nm) wavelengths were selected using bandpass filters and a dichroic mirror.

Mechanical analysis

Tensile tests of unmodified and modified cellulose sheets were performed on an INSTRON 3345 Tensile Tester according to the EN ISO 1924-2 standard. The cross head speed was 2.5 mm/min and the distance between the clamps 180 mm. The samples were rectangular in shape with a width of 15 mm and an approximate thickness of ∼ 0.7 mm.

Thermal analysis

Thermogravimetric (TG) data were acquired between 30 and 300 °C using a Perkin Elmer Diamond thermal analyzer under nitrogen purging gas (100 cm^3min^{-1}) at a heating rate of 10 $Kmin^{-1}$. Differential scanning calorimetry (DSC) analysis was carried out on a Netsch DSC204 instrument under helium flow (30 cm^3min^{-1}) at a heating/cooling rate of 10 Kmin-1. Temperature and enthalpy were calibrated using the melting transition of standard materials (Hg, In, Sn).

RESULTS AND DISCUSSION

Sample morphology

Scanning electron microscope images of cellulose fiber sheets, either unmodified (control) or functionalized by $[Fe(NH_2trz)_3]Br_2$ and $[Fe(Htrz)_2(trz)]BF_4$ particles, are presented in Figure 2. Samples surfaces were investigated in backscattered electron (BSE) mode. In BSE mode the image contrast strongly depends on the atomic number of the constituents in the sample. In contrast to the SEM image of the control sample, the sheets modified by $[Fe(NH_2trz)_3]Br_2$ and the $[Fe(Htrz)_2(trz)]BF_4$ depict a large number of bright objects, which obviously contain heavier atoms than the rest of the matrix. These micrographs basically show that the $[Fe(NH_2trz)_3]Br_2$ and the $[Fe(Htrz)_2(trz)]BF_4$ particles are randomly dispersed over the whole surface of the cellulose fibers, though particle aggregation seems more important in the former case.
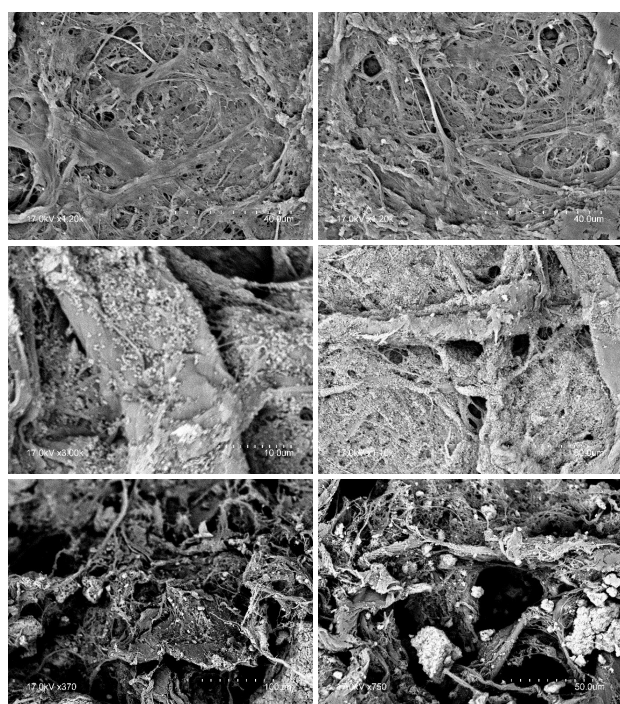

Figure 2. SEM images of unmodified linter fibers (upper panel), composite **1** (middle panel) and composite **2** (bottom panel).

Spectroscopic analysis

Electronic and vibrational spectra were acquired to prove that the composites contain the incorporated SCO particles in the cellulose matrix as well as to test if their structure and spin crossover properties are modified. Figure 3 shows the room temperature diffuse reflectance spectra of the reference cellulose sheet, that of the pure complexes $[Fe(NH_2trz)_3]Br_2$ and $[Fe(Htrz)_2(trz)]BF_4$ as well as that of the modified cellulose fibers in the visible spectral region. Pure linter cellulose fibers lack the structural features required to absorb light in the visible range. The spectra of the four other samples are characterized by a broad absorption band centered at ca. 540 nm. Based on the vast literature on Fe^{II}-triazole SCO complexes [21] we can safely assign this band to the $^1A_1 \rightarrow ^1T_1$

ligand-field transition of the LS form of the complexes. The presence of this absorption band (i.e. the magenta color of the dried handsheets) proves that the iron(II) ions are not oxidized during the elaboration of the handsheets. Due to the relatively low molar absorption coefficient (a few tenths of $M^{-1}cm^{-1}$) associated with this Laporte-forbidden transition it was necessary to load the cellulose matrix with relatively high amounts (ca. 25-30 w%) of thermochromic particles. The room temperature CIELab color space coordinates of the composites are also shown in Figure 3. The L* value of control cellulose (ca. 94) is close to diffuse white (100), while this value decreases in the colored (i.e. LS) state of the composites to ca. 82 indicating increasing optical density. This difference defines basically the print contrast of our inkless paper, which remains moderate, but easily perceptible by eye. The color contrasts (a*, b*) indicate, as can be expected, a change from light yellow to magenta. Positive changes in the a* direction indicate a shift to red color, negative changes from cellulose in b* values represent blue color shift.
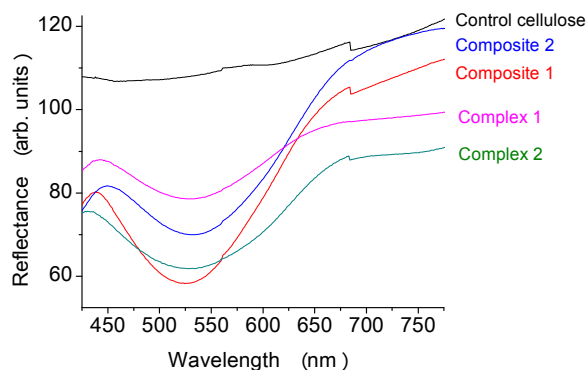
	a*	b*	L*
Cellulose	0.7	4.6	93.78
Composite 1	11.2	-2.7	81.9
Composite 2	6.9	4.1	81.9

Figure 3. UV-vis diffuse reflectance spectrum of unmodified cellulose, the pure complexes and the cellulose composites. The table shows the CIELab coordinates of the unmodified cellulose and those of the two cellulose composites

The spectroscopic fingerprint of the $[Fe(NH_2trz)_3]Br_2$ and the $[Fe(Htrz)_2(trz)]BF_4$ particles as well as that of linter fibers was obtained through vibrational spectroscopic measurements. Figures 4 and 5 show a comparison of the room temperature Raman and FTIR spectra of the reference cellulose sheet, the pure complexes and the composites. The Raman scattering of the cellulose fibers is relatively weak in our experimental conditions and therefore the spectra of the composites arises chiefly from the SCO complexes, though vibrational modes of the cellulose are also observed. On the other hand the FTIR spectra of the composites shows strong absorption of the cellulose fibers superposed with the absorption bands of the SCO complexes. The comparison of the different spectra confirms clearly that the SCO compounds are present in unchanged state in the composite cellulose sheet.
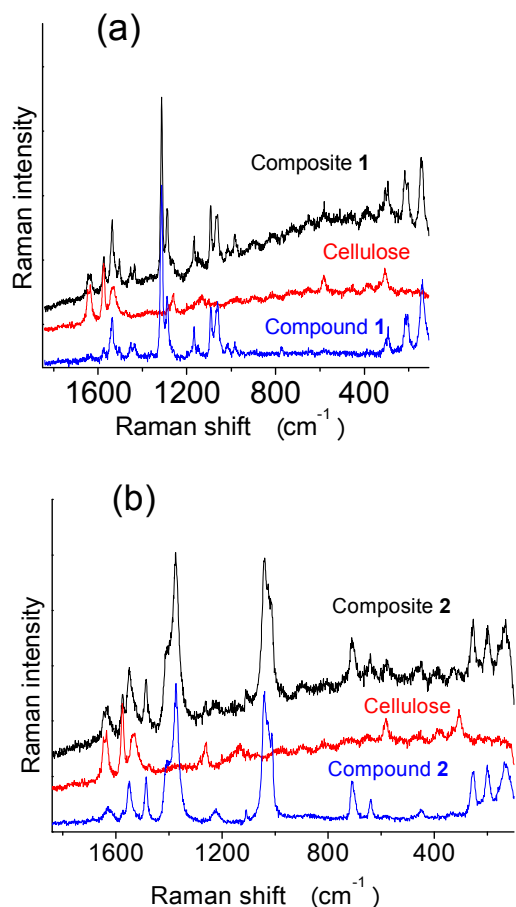
Figure 4. Room temperature Raman spectra (laser power: 0.12 mW) of (a) unmodified cellulose, compound **1** and composite **1**, (b) unmodified cellulose, compound **2** and composite **2**.

Mechanical and thermal properties of the handsheets

The stress-strain curves of the $[Fe(NH_2trz)_3]Br_2$ and $[Fe(Htrz)_2(trz)]BF_4$ modified fibers and the control cellulose handsheets are presented in Figure 6. Overall the composite cellulose sheets show better elongation, lower elastic modulus and reduced resistance to stress. The control cellulose sheets prepared either from EtOH or H_2O suspensions can withstand a stress as high as 12.7 MPa and 12.4 MPa with a 1.9 % and 2.2 % elongation, respectively. The $[Fe(NH_2trz)_3]Br_2$ and $[Fe(Htrz)_2(trz)]BF_4$ treated fiber composite handsheets display significantly lower tensile strength and broke at 4.1 MPa and 5.7 MPa, respectively. On the other hand, the maximum achievable strain of the composite cellulose sheets was ca. 140 % higher than that of the control samples.

The reduced strength and stiffness of the composites can be attributed to the very high loading by SCO particles, which was necessary to obtain a perceptible color change. Nevertheless these data prove that the cellulose/SCO composites indeed show paper-like, self-support properties and can be used without any substrate. The cellulose fiber network appears thus as a good templating

material and reversible printing surface at room and elevated temperature can be achieved. We should note here that the loadings of the composites were not fully optimized neither for the concentration of the particles, neither for their size. It is also possible to use cellulose fiber and/or particle surface modification methods to improve the mechanical properties [22].
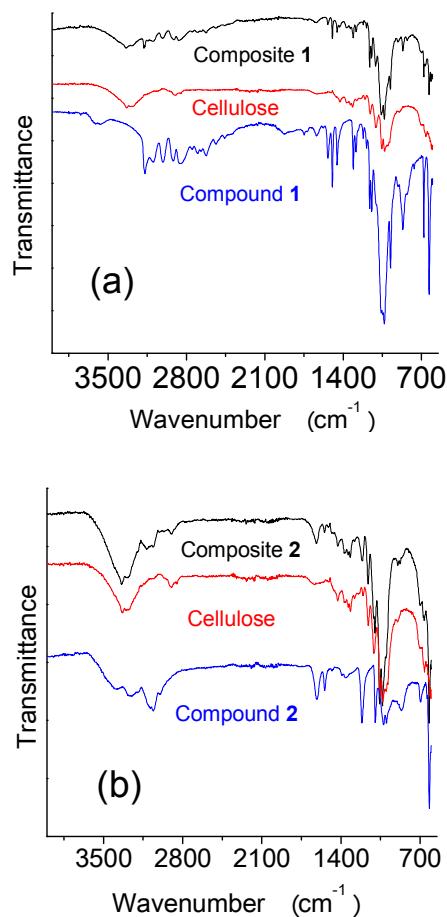

Figure 5. Room temperature FTIR spectra of (a) unmodified cellulose, compound **1** and composite **1**, (b) unmodified cellulose, compound **2** and composite **2**.

The thermal stability (in inert nitrogen atmosphere) of the control and composite cellulose sheets can be depicted from the thermogravimetry data shown in Figure 7. It can be clearly seen that heating the samples up to 100 °C drives off absorbed moisture. Between ca. 100 – 270 °C the control sample exhibits virtually no weight loss. The $[Fe(Htrz)_2(trz)]BF_4$ modified cellulose composite shows nearly similar thermal stability though a slight weight loss (~5 %) occurs already between ca. 170 - 250 °C. The $[Fe(NH_2trz)_3]Br_2$ composite remains stable up to ~220 °C, but above this temperature the thermal degradation escalates. We have not carried out a detailed investigation of the thermal degradation process, but clearly the weight loss in this latter case indicates that

the cellulose fibers are decomposed below 300 °C. We believe that $[Fe(NH_2trz)_3]Br_2$ particles act as catalytic impurities and initiate rapid depolymerization of the cellulose. Oxygen traces in the carrier gas may also contribute to this process. On the other hand, in composite **1** boron atoms might intervene chemically as inhibitors in the oxidation reaction.
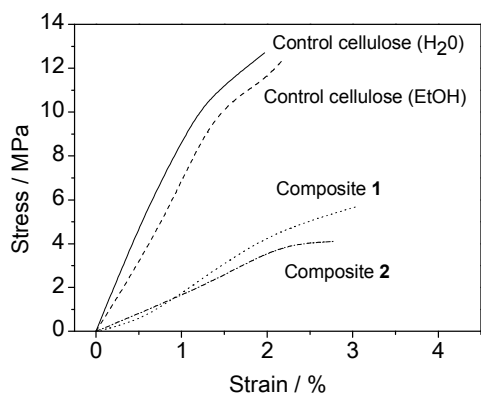

Figure 6. Stress-strain curves of control and composite cellulose handsheets.
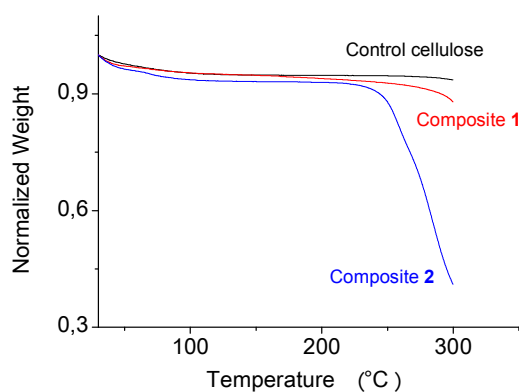

Figure 7. Thermal weight loss of the composite and control papers

The thermal properties of the cellulose composites were further analyzed using DSC (Figure 8). The control cellulose shows only the well-known broad endothermic peak of native cellulose around ca. 80 °C during the first heating, which corresponds to an irreversible structural reorganization [23]. This phenomenon was also observed in the composites. In addition the composites show heat capacity anomalies, which correspond to the latent heat of the spin transition. The corresponding peaks are observed around 111 °C (LS to HS transition upon heating) and 73 °C (HS to LS transition upon cooling) in composite 1 and 35 °C (first heating) 39 °C (second heating) and 33 °C (cooling) in composite **2**. These peaks were found extremely well reproducible upon thermal cycling for composite **1**, while composite **2** displays less stability of the spin transition. In particular we observed a pronounced instability when

this latter composite was heated above ca. 120 °C. The instability of the spin transition in this particular compound is related to polymorphism.
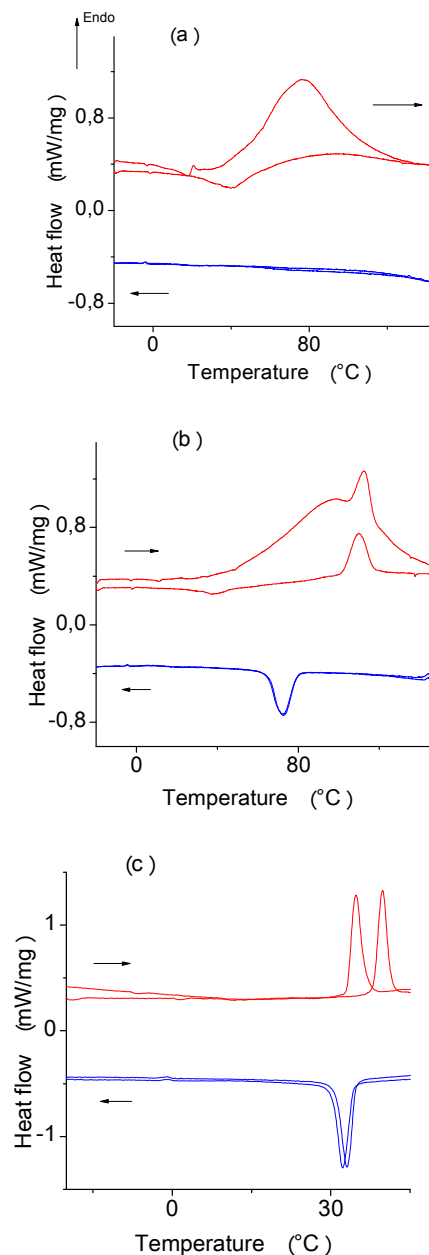

Figure 8. DSC traces of (a) the control cellulose, (b) composite **1** and (c) composite **2** through two successive thermal cycles. (Arrows indicate heating and cooling.)

Thermochromism and printing

The thermal variation of the optical reflectance of the two composites (Figure 9) was followed around 540 nm by cycling the sample between 20 and 45 °C (composite **1**) or between 20 and 120 °C (composite **2**). For comparison the thermochromic response of

This journal is © The Royal Society of Chemistry 20xx

J. Mat. Chem. C, 2015, **00**, 1-3 | **5**

the pure complexes is also shown. The LS to HS spin transition of the $[Fe(NH_2trz)_3]Br_2$ and the $[Fe(Htrz)_2(trz)]BF_4$ complexes upon heating results in the reversible bleaching of the the $^1A_1{\rightarrow}^1T_1$ ligand field absorption band in the visible range. This corresponds to a color change from violet to white. The analysis of the reflectance data reveals that this color change is reversible and occurs rather abruptly around 116 °C (32 °C) in the heating mode and 85 °C (25 °C) in the cooling mode for composite **1** (**2**). Differences with the neat SCO compounds are observed, but these are mainly related to the experimental difficulties to determine accurately the temperature of the handsheets in our experimental setup due to the rather feeble thermal contact with the heater. (N. B. Some difference with the DSC data can be noted also, but this is due to the different heating rates applied in the two experiments.) Nevertheless the observed reflectance changes are unambiguously related to the spin transition process in the $[Fe(NH_2trz)_3]Br_2$ and the $[Fe(Htrz)_2(trz)]BF_4$ complexes as proved by the comparison with the neat compounds.
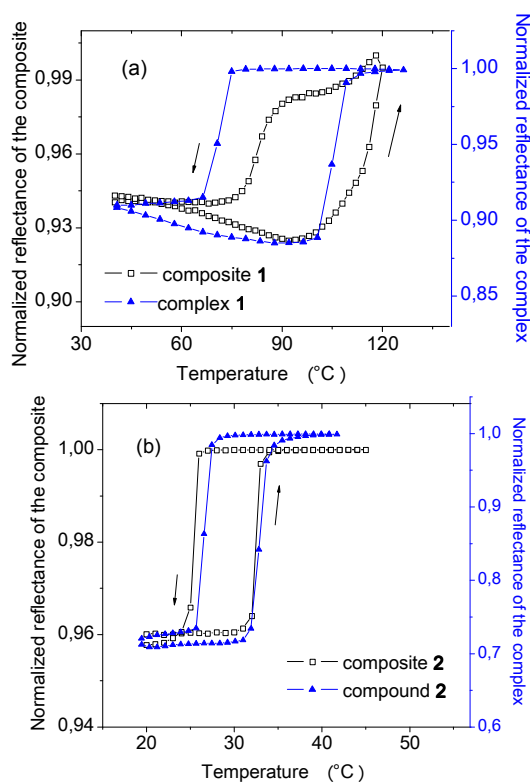

Figure 9. Temperature dependence of the optical reflectance (540 nm) of composite **1** (a) and composite **2** (b) in the heating and cooling modes. The corresponding data of the pure complexes (**1** and **2**) are also shown for comparison. (Arrows indicate heating and cooling.)

As we have discussed in a previous paper [15] the thermochromic properties can be transformed into thermofluorescent properties using an appropriate luminophore. To show this possibility we have elaborated hybrid nanoparticles containing complex **1** and a pyrene-based luminophore [19]. The thermofluorescence response

of these particles embedded in the cellulose matrix are shown in figure 10. The excimer emission of pyrene observed at 550 nm exhibits a significant increase of its intensity when the composite is transformed from its LS to the HS state. This phenomenon is due to the enhanced spectral overlap of the pyrene excimer emission with the LS absorption, but mechanical strain plays also a role [19]. The spin transition temperatures observed through this luminescence modulation are in good agreement with the thermochromic data.
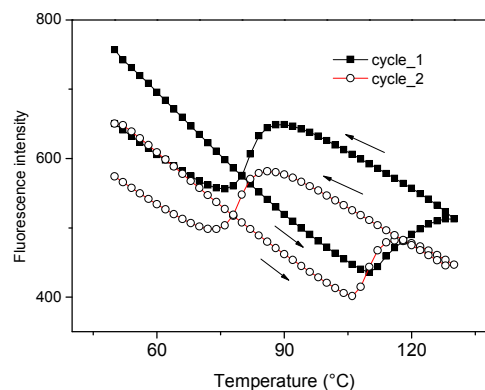

Figure 10. Thermal variation of the fluorescence intensity (excitation: 450 nm, emission: 550 nm) in the heating and cooling modes through two thermal cycles for composite **1** functionalized by pyrene luminophores. (Arrows indicate heating and cooling.)

The thermal hysteresis provides a possibility to store information in the material by local heating or cooling (Figure 11). Within the hysteresis region the free energy of the system exhibits two minima. In the heating (cooling) mode the initially stable LS (HS) state becomes metastable close to the ascending (descending) branch of the hysteresis. Since the lifetime of metastable states in the hysteresis region is very long (virtually infinite) by switching the system from a stable to a metastable state (or vice-versa) the stored information is retained until unwanted heating or cooling occurs beyond the hysteresis temperature region [17]. This well-known idea was recently exploited in polymer-SCO composites [24].
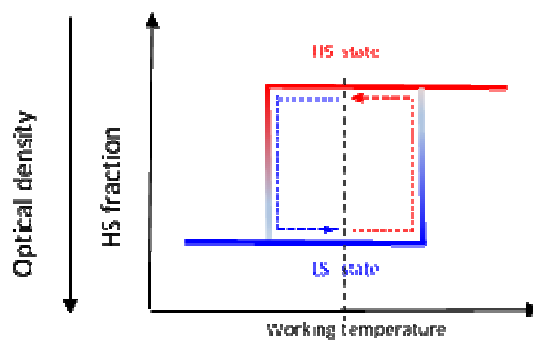

Figure 11. Schematic representation of the memory effect and the thermal printing/erasing cycle

6 | *J. Mat. Chem. C*, 2015, **00**, 1-3

This journal is © The Royal Society of Chemistry 20xx

A simple and efficient way for printing patterns is the use of a focused laser beam, which is raster scanned on the sample to achieve photothermal heating. While relatively slow, this method allows to print point-by-point almost any kind of patterns and the size of the patterns can be relatively small, limited by the diffraction of light as well as by the heat diffusion. We have used the laser beam of our Raman microspectrometer to print patterns into our samples. The particular interest of this approach is that in the same time we can acquire Raman spectra of the exposed area and obtain thus information about the spin state of the composite in the irradiated volume. Figure 12 shows a few selected Raman spectra of the two composites recorded within the heating branch of the thermal hysteresis region using different excitation powers.
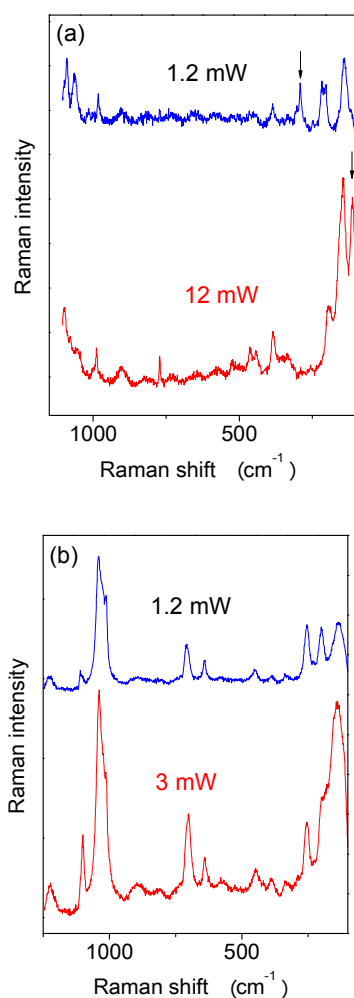

Figure 12. Raman spectra of composite **1** (a) and **2** (b) recorded within the hysteresis region using different laser powers. (The initial state before laser excitation is the LS state, T = 95°C for **1** and 28°C for **2**.)

In these conditions both composites are in the LS state in the absence of laser irradiation. Indeed, for low power excitation we obtained spectra displaying Raman frequencies (290, 208, 140 cm^{-1} for composite **1** and 253, 197, 130 cm^{-1} for composite **2**), which have been unambiguously assigned in previous works to the LS state of these complexes [25-27]. When increasing the laser power above a threshold value a significant change occurs, in particular in the low frequency region of the spectra with the vanishing of the LS marker peaks and the concomitant rise of new peaks around 110 cm^{-1} (composite **1**) and 140 cm^{-1} (composite **2**) characteristic of the HS state. After switching off the laser power the spin state of the complexes remains HS since the temperature of the experiment falls within the hysteresis region.

As shown in figure 13 using the focused laser beam and a motorized sample stage we were able to print very well defined patterns with a linewidth of ca. 150 μm and a position accuracy of a few μm.

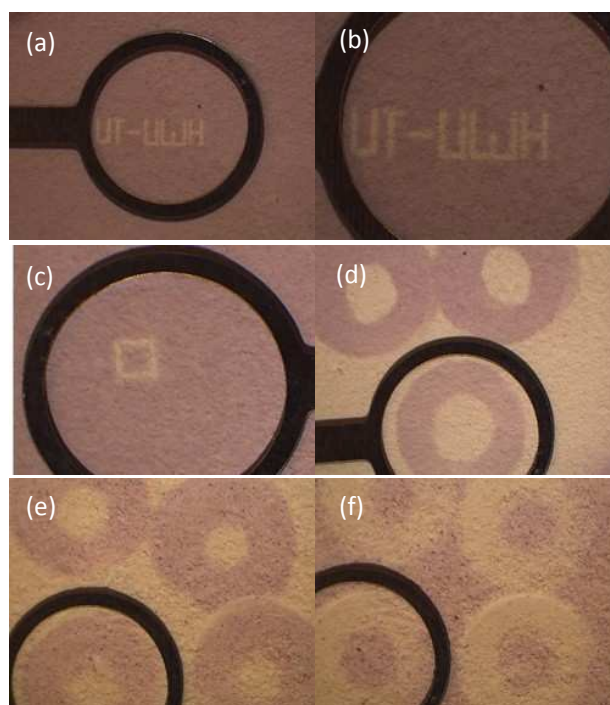Figure 13. Patterns printed by a focused laser beam (a-c) or manually using a stamp (d-f). (**a** - **d**): Composite **1** at 96 °C. (**e** - **f**): composite **2** at 28 °C. Color (LS) prints on white (HS) background and inverse printings are also shown. (The black ring is part of the heating stage: it is used to improve the thermal contact between the sample and the stage.)

It may be worth to note that the diameter of the laser spot in these experiments was approx. 8 μm and it was scanned on the sample surface at a rate of ~10 μm/s. By changing these parameters as well as the laser wavelength (638 nm here) the line width can be adjusted, either broadened or narrowed, within certain limits. Obviously, the laser allows only for heating, but one can also locally heat or cool the handsheets when using a stamp. Figure 13 shows also a few examples for this process. It was possible to print manually violet patterns on the white background by local cooling

ARTICLE   *Journal of Materials Chemistry C*

or, vice versa, to print white patterns on the violet background by local heating using a (hot or cold) metal needle (see also the movie in the Supporting Information). The patterns were easily erasable by heating or cooling of the whole handsheet. The contrast in composite **2** was rather faint due to the partial oxidation of the complex during the elaboration of the handsheets as well as due to their relatively rough surface. On the other hand, the contrast in composite **1** is sharp on both backgrounds (either HS or LS).

The long-term environmental stability and reversibility of the composites is also remarkable. After the elaboration of the handsheets we have carried out a few tenths of printing-erasing cycles. Then we stored the samples during 9 months in ambient conditions (air, daylight, office temperature) and we have not observed any significant degradation of the thermochromism. (Actually, the images shown in figure 13 were acquired after the 9 months storage period.) Subsequently we have carried out more than 100 printing-erasing cycles in ambient air and we were still able to continue to print patterns into both types of papers without any substantial loss of contrast (figure 14). In the case of composite **1** the color of the cellulose matrix becomes yellowish after long exposure to high temperatures in air, but the color change of the complex was clearly observed and we could continue to print into the paper even after 1000 thermal cycles.
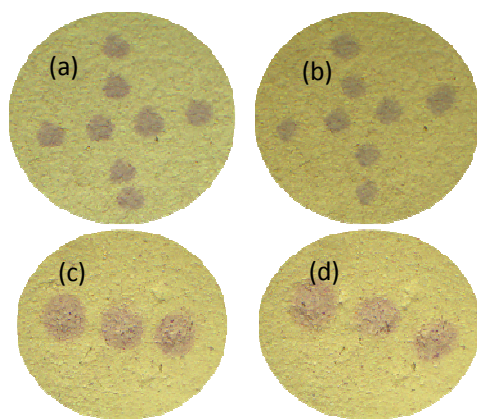

Figure 14. Thermochromism of composite **1** before (a) and after (b) 275 print/erase cycle and that of composite **2** before (c) and after (d) 105 print/erase cycle.

Conclusions

Thermocromic spin-crossover particles were synthesized and mixed with cellulose fibers and fibrils to form a dimensionally stable paper appearance product. Handsheets were produced from these composites according to ISO standards, similar to industry paper-making conditions. This key issue is often overlooked in the literature wherein color-changing dyes are proposed, which are often not compatible with the presence of water or high temperatures associated with the ordinary paper-making process. Parts of our composite papers can be personified by local heating or

cooling to place readable characters in given circumstances. By changing the temperature of the paper the thermally developed characters can be erased and re-personified again. The major advantages of these spin crossover – cellulose composite papers are their short and long term memory capability, good thermal and mechanical stability, homogeneous color, long term stability in ambient storage conditions, compatibility with industrial technologies, low price as well as dye or tonerless reversible printing performance using potentially simple printers, based on heating/cooling. At the present stage of progress these papers have already the potential to be candidates to several applications, such as anticounterfeit paper products, dynamic-reversible inkless paper, learning materials and paper thermometer. Even more importantly this work provides a proof of concept for the possibility to achieve a reversible, printable, inkless paper using the thermal hysteresis exhibited by certain spin-crossover compounds. However, the different and very stringent requirements for this application have not yet been met in a single compound. Compound **2** works near room temperature, but the hysteresis width is not sufficiently large for information storage. On the other hand compound **1** exhibits a sufficiently large and very robust hysteresis for applications, but the spin transition occurs at high temperature. Undoubtedly there is no fundamental reason why not to find a spin crossover compound, which exhibits all the necessary attributes (large hysteresis, room temperature operation, environmental stability and reversibility) for a potentially very attractive inkless paper product. The problem is that the spin transition properties are not predictable at present and the search for this compound must be based to a large extent on serendipity – even if a few known synthetic strategies can be useful to this aim [17, 28]. The only - though not the least - fundamental problem concerns color and optical density. These are related chiefly to the ligand field of the complex in the LS state, which is restricted to a narrow range by the need for a spin transition at room temperature [29]. One might consider the use of charge transfer absorption bands, whose energy may be tuned perhaps slightly more easily and which are associated with much higher optical densities. Clearly, a lot of work remains until a viable solution can be obtained, but we believe that the expected economic and environmental benefits do justify these efforts.

Supporting information.

Movie of a print/erase cycle. This material is available free of charge via the Internet at http://pubs.rsc.org.

REFERENCES

1   W.H. Banks, Paper in the printing process. Pergamon press: Oxford, 1967.
2   W. Wang, N. Xie, L. He, Y. Yin, *Nat. Commun*. 2014, **5**, 5459.
3   H. Fudouzi, Y.N. Xia, Adv. Mater. 2003, **15**, 892–896.
4   J. Ge, J. Goebl, L. He, Z. Lu, Y. Yin, *Adv. Mater*. 2009, **21**, 4259–4264.
5   A. Kishimura, T. Yamashita, K. Yamaguchi, T. Aida, *Nat. Mater*. 2005, **4**, 546–549.
6   R. Klajn, P.J. Wesson, K.J.M. Bishop, B.A. Grzybowski, *Angew. Chem. Int. Ed.* 2009, **48**, 7035–7039.

7   J.J. Zhang, Q. Zou, H. Tian, *Adv. Mater.* 2013, **25**, 378–399.
8   Y. Kohno, Y. Tamura, R. Matsushima, *J. Photochem. Photobiol. A.* 2009, **201**, 98–101.
9   I. Kawashima, H. Takahashi, S. Hirano, R. Matsushima, *J. Soc. Inf. Display*. 2004, **12**, 81–85.
10 J. Garcia-Amoro´s, S. Swaminathan, F. M. Raymo, *Dyes Pigments* 2014, **106**, 71–73.
11 L. Sheng, M. Li, S. Zhu, H. Li, G. Xi, Y.G. Li, Y. Wang, Q. Li, S. Liang, K. Zhong, S.X.A. Zhang, *Nat. Commun.* 2014, **5**, 3044.
12 D.A. Hays, *J. Electrostat*. 2001, **51**, 57–63.
13 T. Horiguchi, Y. Koshiba, Y. Ueda, C. Origuchi, K. Tsutsui, *Thin Solid Films*. 2008, **516**, 2591–2594.
14 S. Yamamoto, H. Furuya, K. Tsutsui, S. Ueno, K. Sato, *Cryst. Growth Des.* 2008, **8**, 2256–2263.
15 V. Nagy, K. Halász, M-T. Carayon, I.A. Gural'skiy, S. Tricard, G. Molnár, A. Bousseksou, L. Salmon, L. Csóka, *Coll. Surf. A: Phys. chem. Eng. Aspects*. 2014, **456**, 35-40.
16 P. Gütlich, A. Hauser, H. Spiering, *Angew. Chem. Int. Ed.* 1994, **33**, 2024-2054.
17 O. Kahn, C.J. Martinez, *Science.* 1998, **279**, 44-48.
18 J. Kröber, J-P. Audiere, R. Claude, E. Codjovi, O. Kahn, J.G. Haasnoot, F. Grolière, C. Jay, A. Bousseksou, J. Linares, F. Varret, A. Gonthier-Vassal, *Chem. Mater*. 1994, **6**, 1404-1412.
19 I. Suleimanov, O. Kraieva, J. Sanchez Costa, G. Molnár, L. Salmon, I.O. Fritsky, A. Bousseksou, *J. Mater. Chem. C* 2015, in press.
20 L.G. Lavrenova, V.N. Ikorskii, V.A. Varnek, I.M. Oglezneva, S.V. Larionov, *Koord. Khim.* 1986, **12**, 207-215.
21 O. Roubeau, *Chem. Eur. J.* 2012, **18**, 15230-15244.
22 Z. Zheng, J. McDonald, R: Khillan, Y. Su, T. Shutava, G. Grozdits, Y.M. Lvov, *Nanosci. Nanotechnol*. 2006, **6**, 624-632.
23 P.K. Chatterjee, *J. Appl. Polym. Sci.* 1968, **12**, 1859-1864.
24 W. Hellel, A. Ould Hamouda, J. Degert, J. F. Létard, E. Freysz, *Appl. Phys. Lett.* 2013, **103**, 143304.
25 Y.A. Tobon, L. Kabalan, S. Bonhommeau, N. Daro, A. Grosjean, P. Guionneau, S.F. Matar, J-F. Létard, F. Guillaume, *Phys. Chem. Chem. Phys.* 2013, **15**, 18128-18137.
26 N. Ould Moussa, D. Ostrovskii, V. Martinez Garcia, G. Molnár, K. Tanaka, A.B. Gaspar, J.A. Real, A. Bousseksou, *Chem. Phys. Lett*. 2009, **477**, 156-159.
27 F. Guillaume, Y.A. Tobon, S. Bonhommeau, J-F. Létard, L. Moulet, E. Freysz, *Chem. Phys. Lett*. 2014, **604**, 105-109.
28 I. Salitros, N.T. Madhu, R. Boca, J. Pavlik, M. Ruben, *Monatsh. Chem*. 2009, **140**, 695-733.
29 A. Hauser*, Top. Curr. Chem*. 2004, **233**, 49-58.